CHEMISTRY
AN ASIAN JOURNAL
www.chemasianj.org

Accepted Article

Title: Constructing ordered three-dimensional channels of TiO2 for enhanced visible-light photo-catalytic performance of CO2 conversion induced by Au nanoparticles

Authors: Hairong Xue, Tao Wang, Hao Gong, Hu Guo, Xiaoli Fan, Bin Gao, Yaya Feng, Xianguang Meng, Xianli Huang, and Jianping He

To be cited as: *Chem. Asian J.* 10.1002/asia.201701807

Link to VoR: http://dx.doi.org/10.1002/asia.201701807

A Journal of
ACES Asian Chemical Editorial Society

A sister journal of Angewandte Chemie and Chemistry – A European Journal

WILEY-VCH

10.1002/asia.201701807

WILEY-VCH

Constructing ordered three-dimensional channels of TiO_2 for enhanced visible-light photo-catalytic performance of CO_2 conversion induced by Au nanoparticles

Hairong Xue,[a,b] Tao Wang,*[b] Hao Gong,[b] Hu Guo,[b] Xiaoli Fan,[b] Bin Gao,[b] Yaya Feng,[b] Xianguang Meng, [c] and Jianping He*[b]

Abstract: As a typical photo-catalyst for CO_2 reduction, the practical application of TiO_2 still suffers from low photo-catalytic efficiency and limited visible light absorption. Here, a novel Au-nanoparticle (NP)-decorated ordered mesoporous TiO_2 (OMT) composite (OMT-Au) was successfully fabricated, in which Au NPs uniformly disperse on the OMT. Due to the surface plasmon resonance (SPR) effect derived from the excited Au NPs, TiO_2 possesses high photo-catalytic performance for CO_2 reduction under visible light. The ordered mesoporous exhibits the superiority of material and structure. This ordered mesoporous structure of TiO_2 with a high surface area offers more catalytic activity sites. More importantly, the three-dimensional transport channels ensures smooth flow of gas molecules, high-efficient adsorption ability of CO_2, and the fast and steady transmission of hot electrons excitation on Au NPs, thus leading to further improving photo-catalytic performance. These results highlight the possibility of improving visible light photo-catalysis for CO_2 reduction by constructing OMT-based Au-SPR-induced photo-catalysts.

Introduction

Photo-catalytic CO_2 reduction has attracted increasing research attention due to its tremendous potential in solving environmental and energy crisis, which provides a renewable approach for producing the valuable hydrocarbon compounds.[1-7] Normally, CO_2, as an oxidized form of carbon, is very stable and difficult to be activated in the reduction process.[8] For this challenge of CO_2 conversion, various semiconductor photo-catalysis have been explored to accelerate the photo-catalytic CO_2 conversion.[9-13] Thereinto, TiO_2 is a typical wide-band gap semiconductor, which has served as the most common photo-catalysts in photo-catalytic CO_2 reduction.[14] However, the practical application of TiO_2 still suffers from some major constraints, including significant photo-catalytic efficiency loss and limited absorption of visible light photos.[15-18] Recently, because of high specific surface area and plentifully interconnected porous network, some mesoporous photo-catalysts have been explored for photo-catalysing CO_2 reduction.[19-22] In addition, compared with the photo-catalysts with disordered mesoporous structure, intensive research efforts shown that ordered mesoporous materials can effectively separate photo-induced electrons and facilitate the diffusion of reactants, thus leading to enhanced photo-catalytic activity.[23-30] Therefore, benefiting from ordered mesoporous channels and uniformly distributed porosity, ordered mesoporous TiO_2 shows the high potential as a promising candidate for photo-catalysis in conversion of CO_2.

Although the photo-catalytic activity of TiO_2 for CO_2 reduction can be effectively improved by constructing ordered mesoporous structure, the utilization of solar energy still should be increased. As a cutting-edge research field, it was discovered that plasmonic photo-catalysis originated from the surface plasmon resonance (SPR) has been applied in CO_2 reduction, organic transformation, and environmental, served as a visible-light photo-catalysis.[31-39] Based on the SPR of plasmonic-metal NPs (e.g., Au), their surface electrons can collectively oscillate induced through the resonant photon, simultaneously energetic hot electrons are produced by non-radiative excitation[33,40]. In the SPR process, because of the short lifetime of the hot electrons (~ 10^{-3} ns), a semiconductor are often used in conjunction with plasmonic-metal NPs.[40-41] Due to the hot electron injection into a semiconductor, lifetime of the hot electrons can be effectively extended (~10^0 ns).[40,42-43] For this plasmonic-metal NPs/semiconductor composite, it is shown that the conduction band (CB) of the semiconductor can be injected with the hot electrons of plasmonic-metal NPs over the Schottky barrier, which can intrinsically drive the visible-light photo-catalysis[40]. Over the past few years, some researches have shown that the semiconductors incorporated with plasmonic-metal nanoparticles (NPs) shown enhanced visible-light absorption, which was beneficial to overcome the limitation of photo-absorption.[44-46] For example, plasmonic Au/TiO_2 photo-catalyst has been reported that H_2 generation rate can be significantly increased under visible light irradiation in alkaline reaction environment, benefiting from the effectively suppressive recombination of holes and hot electrons through fast consumption of the holes in Au NPs.[44] Moreover, when BiOCl nanosheets are modified with Au NPs to construct plasmonic photo-catalyst, the Au-induced high aerobic oxidation activity for 2-propanol under visible-light can be obtained due to the more efficient hot-electron transfer.[45] In both water oxidation and iso-propanol degradation, Au–$SrTiO_3$–TiO_2 photo-catalyst possesses multicomponent junction nanostructure, which exhibits the effectively enhanced Au-induced photo-catalytic

[a] Dr. H. Xue
College of Chemical Engineering, Zhejiang University of Technology Hangzhou, Zhejiang 310014, P.R. China.
[b] Prof. Dr. T. Wang,* H. Gong, H. Guo, X. Fan, B. Gao, Y. Feng, Prof. Dr. J. He*
College of Materials Science and Technology, Jiangsu Key Laboratory of Materials and Technology for Energy Conversion, Nanjing University of Aeronautics and Astronautics, Nanjing 210016, P.R. China.
E-mail: wangtao0729@nuaa.edu.cn; jianph@nuaa.edu.cn.
[c] Prof. Dr. X. Meng
Photo-functional Materials Research Platform, College of Materials Science and Engineering, North China University of Science and Technology, Tangshan 063210, P.R. China.
Supporting information for this article is given via a link at the end of the document.

performance under visible light.[46] Obviously, both plasmonic-metal NPs and semiconductor are two indispensable counterparts of the plasmonic photo-catalysts. During a long period in the past, the intense investigation of these photo-catalysts focus on the function of the plasmonic-metal NPs, such as sizes, shapes and so on.[31-32,47-48] In contrast, there is much less attention for the semiconductor, which is used as a hot electron acceptor. Until recently, for the plasmonic photo-catalysts, the essential role of semiconductor materials was preliminarily recognized, some researchers began to explore the relationship between the photo-catalytic activity and structure of the semiconductor.[44-46] Compared with the common TiO_2 NPs, mesocrystal TiO_2 can accumulate more hot electrons within a much shorter time in the SPR process, thus leading to the longer lifetime and enhanced photo-catalytic activity of the Au-SPR-induced photo-catalysts. In order to develop and design efficient Au-induced visible-light photo-catalysts, the modification of the semiconductor should be one of great importance.

Herein, we report the Au-SPR-induced photo-catalytic performance under visible-light in CO_2 reduction can be effectively improved by constructing an ordered mesoporous TiO_2-Au (OMT-Au) plasmonic photo-catalyst. Compared with commercial TiO_2 nanopowders-Au (P25-Au) and disordered mesoporous TiO_2-Au (MT-Au), the photo-catalytic activity for CO_2 reduction of OMT-Au is much higher due to the high specific surface area and ordered channel structure of OMT. In addition, charge separation of OMT-Au is more efficient and electron transport across the OMT-Au junction is also much fast. As a result, for OMT-Au, the total reduced rate (CH_4 + CO) is 10 and 7 times higher than those obtained over P25-Au and MT-Au, respectively. More importantly, based on $^{13}CO_2$ detection technique, the C atoms of CH_4 have been confirmed that they are from CO_2. These results indicate that rational design and fabrication of OMT–Au can be an attractive method to develop efficient Au-SPR-induced photo-catalysts for CO_2 reduction under visible-light.

Results and Discussion

Figure 1 displays the designed route for the preparation of OMT-Au composite, which is synthesized by an EISA strategy combined with impregnation-reduction method. Before the EISA process, soft-template agent (F127), “binder” (phenolic resol precursor) and metal salts (tetrabutyl titanateare) are uniformly dissolved into ethanolic solution, which can co-assemble into nanorod-like micelles. Subsequently, the obtained orange colour solution is transferred into culture dish, followed by evaporation of the ethanol solvent (room temperature) and thermal polymerization (100 ºC). After thermosetting, the obtained dark green film is further treated by thermal treatment (350 ºC) in N_2 atmosphere, then the F127 template will be remove to form a stable puce polymer-Co-TiO_2. Then, well-crystallized TiO_2 with ordered mesoporous structure can be formed after removing organics, heated at 400 ^{o}C in air. During the impregnation process, a part of gold salt precursor can impregnate into the channels of OMT through capillary action, meanwhile, another part can cover on the surface of OMT. Finally, Au-incorporated OMT composite can be successfully synthesized by the reducing action of ascorbic acid, in which the Au NPs uniformly distribute into the channels or on the surface of OMT.

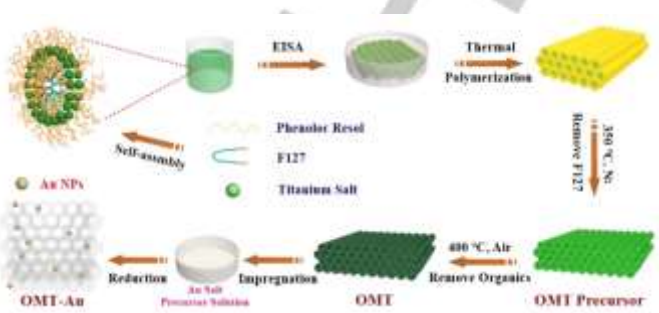

Figure 1. Schematics showing preparation of OMT-Au composite.

The XRD patterns of OMT-Au, MT-Au and P25-Au composites are shown in Figure 2(a), characterized their crystalline structure. As shown in Figure 2(a), there are several intensity diffraction peaks of the three samples in the XRD patterns, which are all in accord with the standard card (JCPDS no. 21-1272) of anatase phase TiO_2. In addition, it also can be found some well-defined characteristic XRD peaks of Au (JCPDS no. 01-089-3697). This result shows the successful synthesis of the TiO_2 based Au-SPR-induced photo-catalysts. By using N_2 adsorption-desorption isotherms, we can analyze the pore structure of the three samples. According to the IUPAC classification, type IV isotherm can be observed in all samples shown in Figure 1(b), suggesting that all samples have the typical mesoporous structure.[49-50] Furthermore, it is noteworthy that OMT-Au composite shows a H1-type hysteresis loop and an obvious N_2 uptake occurring at P/P_O of 0.4-0.7, indicating the one-dimensional cylindrical channels existed in the mesoporous materials. For MT-Au and P25-Au composites, they all show H3-type hysteresis loops, which are associated with the slit-shaped pores derived from the aggregation of plate-like NPs. Figure 2(c) describes the pore-size distribution curves of the samples. The curve illustrates that OMT-Au composite possesses a narrow pore-size distribution. Moreover, as shown in Table 1, the OMT-Au composite exhibits the highest specific surface area, desirable pore volume and the largest pore size, calculated by using BET method and BJH model. Therefore, we infer that structural features of the OMT-Au composite provide many advantages for improving the photo-catalytic performance under visible-light in conversion of CO_2. The higher specific surface area can offer more catalytic activity sites for photo-catalysis. At the same time, desirable pore volume and large pore size are beneficial to sufficient infiltration of electrolyte to obtain facile ion transportation.

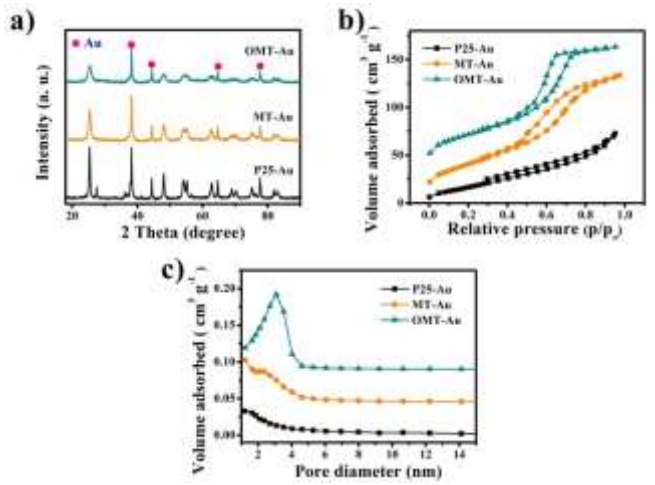

Figure 2. (a) The XRD patterns; (b) N_2 adsorption/desorption isotherms; (c) pore size distribution curves of OMT-Au, MT-Au and P25-Au composites.

Table 1. Pore-structure parameters of OMT-Au, MT-Au and P25-Au composites.

Sample	$S_{BET}/m^2 \cdot g$	$V_{total}/cm^3 \cdot g$	D/nm
OMT-Au	181	0.26	5.8
MT-Au	148	0.21	5.5
P25-Au	72.9	0.11	6.2

The particle size, dispersibility and crystallinity of OMT-Au, MT-Au and P25-Au composites can be characterized by SEM and TEM measurement. As shown in Figure 3(a), the OMT-Au composite exhibits an obviously ordered mesoporous structure of TiO_2, and the Au NPs uniformly distribute on the surface of OMT. Moreover, the ordered parallel mesoporous channel of the OMT-Au composite can be clearly seen in Figure 3(c), whose pore-size is estimated to be ~5 nm. The HRTEM images (I) (inset of Figure 3(c)) and Figure S1 further confirms the ordered mesoporous structure of TiO_2, which is made up of the abundant high crystalline TiO_2 NPs with a diameter of 5~10 nm. It also can be found that Au NPs with the particle size of 20~25 nm possesses the high crystallization, evidenced by their clear lattice fringes calculated to be ~0.235 nm, corresponding to the interlayer spacing of Au (111) facets. The evenly distribution of Ti, O and Au elements in the OMT-Au NPs was described by the EDX elemental mappings (Figure 3(e)), indicating the successful combination between OMT and Au NPs. Contrastively, Although MT-Au composite also can successfully combine with Au NPs, it shows the disordered mesoporous structure of TiO_2. For P25-Au composite, it consists of TiO_2 NPs and the particle size of TiO_2 is around 20~30 nm (Figure S2, Supporting Information). Therefore, these results show OMT-Au composite has an ordered mesoporous structure of TiO_2, high crystallization of NPs and uniform distribution of Au NPs, which are beneficial to enhancing the visible-light photo-catalytic performance for CO_2 reduction.

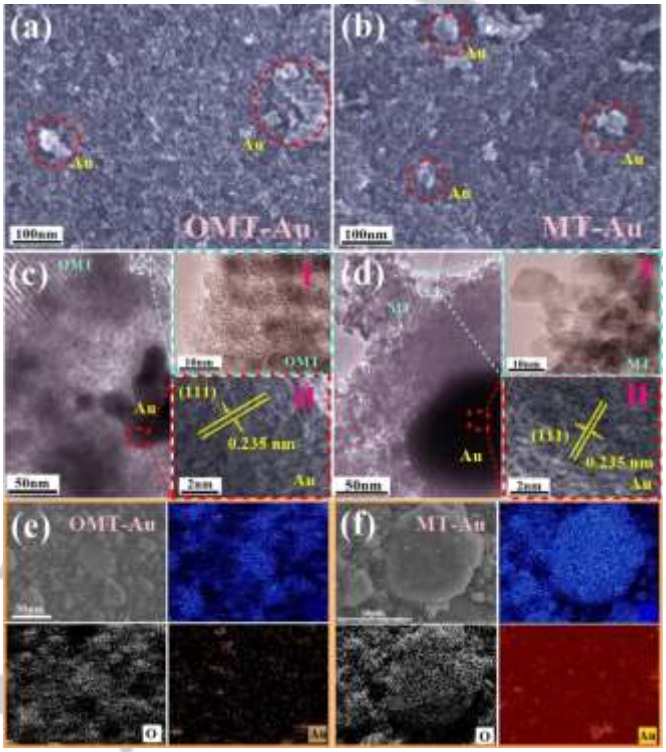

Figure 3. (a,b) FESEM images; (c,d) TEM images; (e,f) STEM and EDX mapping images of OMT-Au and MT-Au composite. (a,c,e): OMT-Au; (b,d,f): MT-Au.

Figure 4(a) shows the UV-visible spectra of the OMT-Au, MT-Au and P25-Au photo-catalysts. It can be seen that all photo-catalysts exhibits typical absorption peaks in the 520-560 nm wavelength range. As we all know, TiO_2 served as a photo-catalyst shows no response under visible-light. Therefore, these above mentioned absorption peaks are attributed to the existence of the Au NPs, which suggests that the hot electrons can accumulate in TiO_2 during the SPR process. We carried out the CO_2 photo-reduction reaction under visible light in a gas-closed circulation system, in the presence of water vapor, CO_2, and photocatalysts. As shown in Figure 4(b) and (c), similar to a lot of reports,[4,51] the CO_2 is reduced to CH_4 and CO, and the amounts of products for OMT-Au are larger than the amounts of products for MT-Au and P25-Au. The generated rates of CH_4 and CO over the photocatalysts were calcuted according to the amounts evolved in 6 h (Figure 4(d)). The generated rates of CH_4 over OMT-Au, MT-Au and P25-Au are 0.33, 0.28, and 0.21 $\mu mol\ g^{-1}\ h^{-1}$, respectively. The generated rate of CO over OMT-Au is 1.83 $\mu mol\ g^{-1}\ h^{-1}$, while the amount of CO generated on P25-Au and MT-Au was negligible. For CO_2 reduction, the overpotential of CH_4 evolution is much smaller than that of CO evolution. So, compared with CH_4 evolution, the generated rate of CO over OMT-Au is much higher than those of MT-Au and

P25-Au, due to its higher photo-catalytic activity. The total reduced rate (CH_4 + CO) of CO_2 over OMT-Au is 7 times higher than the MT-Au, and 10 times higher than the P25-Au. Furthermore, as shown in Figure 4(b), after 10 h, both of the generated rates of CH_4 on P25-Au and MT-Au rapidly reduce, but the generated rates of CH_4 on OMT-Au is still stable. In our previous studies, we demonstrated that the better ordered mesostructure of TiO_2 is, the higher photo-catalytic activity and stability for reduction of CO_2.[21-22] The isotopic analysis of carbon was necessary and conducted by using $^{13}CO_2$ to replace $^{12}CO_2$. The products were analyzed in the GC-MS spectrum. As shown in Figure S3(a) and (b) (Supporting Information), the peaks with the retention time 02:10 and 02:22 are confirmed to be the products ^{13}CO (named X) and $^{13}CH_4$ (named Y) for OMT-Au. The intensity ration of X^+ and $(X-13)^+$ of ^{13}CO (*m/z=29, 16*) matched that of CO (*m/z=28, 16*), and the intensity ration of Y^+, $(Y-1)^+$ and $(Y-2)^+$ of $^{13}CH_4$ (*m/z=17, 16, 15*) matched that of $^{12}CH_4$ (*m/z=16, 15, 14*). The result of the GC-MS spectrum for $^{12}CO_2$ reduction is similar to that of $^{13}CO_2$ reduction (Figure S4(a,b)). That is to say, the products CO and CH_4 are proved to be changed from the reduction of CO_2. In consequence, the OMT-Au composite is a promising choice, served as an efficient Au-SPR-induced photo-catalyst for CO_2 reduction under visible-light.

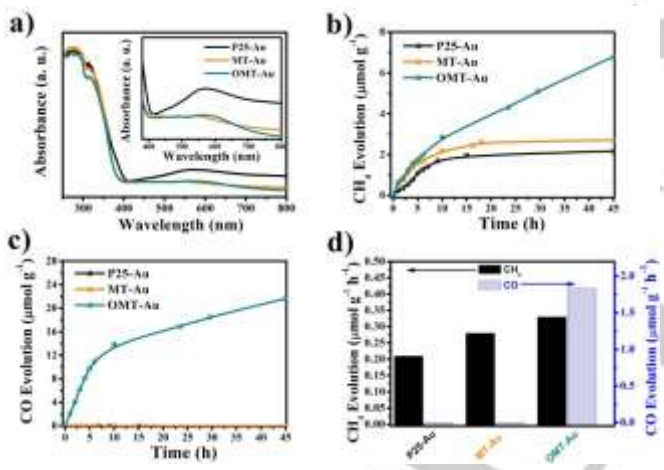

Figure 4. (a) UV-vis absorption spectra and differential spectra (inset); (b) CH_4 and (c) CO evolutions under visible light irradiation over OMT-Au, MT-Au and P25-Au photo-catalysts; (d) Comparison of photo-catalytic activity of OMT-Au, MT-Au and P25-Au photo-catalysts.

Figure 5 shows a schematic illustration of CO_2 photo-reduction through the SPR of Au NPs under visible light. Based on the results of UV-visible spectra, this reaction process involves two stages. On the one hand, under visible light illumination, collective oscillation of electrons can produce hot electrons by the excitation of SPR on Au NPs. Compared with Schottky barrier energy ϕ_{SB}, the energies of hot electrons is higher, so these hot electrons can be injected into the conduction band of semiconductor (TiO_2). Simultaneously, the holes can leave in the Au NPs. On the other hand, the hot electrons injected into TiO_2 can contribute to reduction of CO_2. Meanwhile, the holes in the Au NPs can contribute to the oxidation of H_2O. Therefore, the combination of TiO_2 and Au NPs can potentially improve the photo-catalytic performance under visible-light in conversion of CO_2. Notably, CO_2 reduction occurs at the semiconductor, so the photo-catalytic activity and stability of the TiO_2 have an important influence on the photo-catalytic performance for CO_2 reduction. In this work, OMT-Au composite as a plasmonic photo-catalyst shows excellent photo-catalytic performance mainly benefits by structural and material superiorities. The structural features and photo-catalytic CO_2 reduction mechanism of OMT-Au composite is shown in Figure 5. As a photo-catalyst, this ordered mesoporous TiO_2 with the high specific surface area provides more reaction sites, which exist both on the TiO_2 NPs surface and in the pores. Furthermore, this highly ordered mesoporous structure of TiO_2 can harvest more light due to the multiple scattering. Their continuous pore channels ensure smooth flow of gas molecules and high-efficient adsorption ability of CO_2. Moreover, three-dimensional network formed from the porous TiO_2 framework is beneficial to the fast and steady transmission of hot electrons, thus leading to the enhanced separation/transport of electron-hole. For MT-Au and P25-Au, because of the presence of Au NPs, hot electrons also can be produced by the excitation of SPR on Au NPs. However, either P25 or MT shows the lower the photo-catalytic activity and stability, due to the absence of the structural features of OMT. Therefore, the photo-catalytic activity for CO_2 reduction of OMT-Au is much higher than that of MT-Au and P25-Au. As a new Au-SPR-induced photo-catalyst, OMT-Au shows a remarkable photo-catalytic performance for CO_2 reduction under visible light.

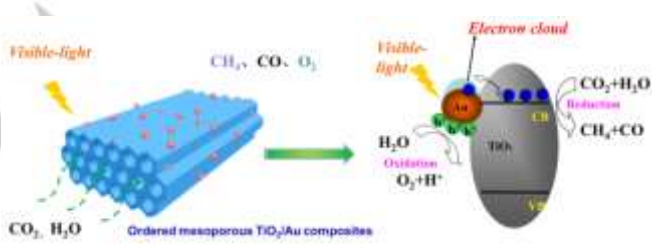

Figure 5. Possible mechanism of OMT-Au photo-catalysts in CO_2 reduction.

Conclusions

We have successfully fabricated a novel Au-nanoparticle-decorated ordered mesoporous TiO_2 composite (OMT-Au) by using a multi-constituents co-assembly strategy combined with impregnation-reduction method. For OMT-Au composite, TiO_2 possesses high photo-catalytic performance for CO_2 reduction under visible light, due to the Au-induced SPR effect. Moreover, photo-catalytic performance of OMT-Au composite can be further improved, profiting from the ordered mesoporous structure of TiO_2. The smooth flow of gas molecules, high-efficient adsorption ability of CO_2, and the fast and steady transmission of hot electrons can be obtained by the high surface area and three-dimensional transport channels of OMT.

Finally, for, the total reduced rate (CH_4 + CO) of OMT-Au composite is 10 and 7 times higher than those obtained over P25-Au and MT-Au, respectively. More importantly, based on $^{13}CO_2$ detection technique, the C atoms of CH_4 have been confirmed that they are from CO_2. Therefore, design and preparation of OMT-based Au-SPR-induced photo-catalysts is a promising pathway to improving photo-catalysis for CO_2 reduction under visible light.

Experimental Section

Preparation of OMT and MT composites:

The well-crystallized ordered mesoporous TiO_2 was by evaporation induced self-assembly process, following the two-step calcination processes. Typically, of triblock copolymer Pluronic (2.0 g) was poured into ethanol (20.0 mL) at 40 °C. After vigorous stirring for 1 h, soluble resol (2.5 g) and tetrabutyl titanate (3.4 g) were added into above solution under vigorous stirring for 2 h. The solution was poured into Petri dishes and kept at 100 °C for 24 h in an oven. The obtained film was then carbonized in the N_2 atmosphere at 350 °C for 4 h, by using a heating rate of 1 °C min^{-1}. Finally, the ordered mesoporous TiO_2 was calcined at 400 °C for 5 h under air atmosphere with a heating rate of 1 °C min^{-1}. The disordered mesoporous TiO_2 can be obtained by using the similar synthesis of OMT without adding soluble resol, named as MT.

Preparation of OMT-Au, MT-Au and P25-Au composites:

Typically, potassium chloroaurate was dissolved into distilled water. This homogeneous transparent solution was dropwise added into the as-prepared OMT powder. Subsequently, excessive ascorbic acid aqueous solution was further dropwise added into above OMT powder. During drying in the vacuum oven, almost all of gold salt precursor was converted into Au NPs, due to the reducibility of excessive ascorbic acid. After drying, Au NPs-ordered mesoporous TiO_2 composite with around 5 wt.% of Au content was formed, marked as OMT-Au. The preparation of disordered mesoporous TiO_2-Au NPs and commercial P25-Au NPs was similar to the OMT-Au, marked as MT-Au and P25-Au, respectively.

Structural and morphological characterization:

An X-ray diffractometer (Bruker D8 Advance) was used to obtain the X-ray diffraction (XRD) patterns, using a Cu Ka source on. The pore size distributions and specic surface areas of the samples were measured on Micromeritics ASAP 2010 by Nitrogen adsorption–desorption isotherms at 77 K. The field-emission-scanning electron microscope (Hitachi S-4800) was used to record the scanning electron microscopy (SEM) images. The field-emission transmission electron microscope (JEOL JEM-2100) was used to observe the morphology. Then the elements of microzone composition were analyzed by energy dispersive X-ray spectrometer (EDX) installed in a 2100F (STEM-EDX mapping). The UV-visible spectrophotometer (UV-2600; Shimadzu Corp., Japan) was used to test the diffuse refection spectra of the samples. Then, based on the Kubelka–Munk equation, the absorption spectra were transformed from the reflectance spectra.

2.3 Photocatalytic measurements:

Before the photo-catalytic reaction, in order to remove organic adsorbates, the three samples were treated in air (200 °C, 48 h). An airtight circulation system was used to test the photo-reduction of CO_2, in which the light source is a 300 W xenon arc lamp equipped with a glass filters (L-42). After uniformly dispersing the sample (0.1 g) on a porous quartz fiber filter film in the reaction cell, the deionized H_2O (3 mL) was injected into the airtight system and then the pure CO_2 gas (80 kPa) was also introduced. A gas chromatograph (GC-14B, Shimadzu Co., Japan) was used to measure the products. The isotope experiments of ^{13}C were performed by using a gas chromatographmass spectrum (JEOL-GCQMS, JMS-K9 and 6890N Network GC system, Agilent Technologies). The isotopic analysis of ^{13}C was conducted by using $^{13}CO_2$ to replace $^{12}CO_2$, and its process is the same as $^{12}CO_2$.

Acknowledgements

This research was sponsored by the Natural Science Foundation of Jiangsu Province (BK20160795), the National Natural Science Foundation of China (51602153, 11575084, and 21703065), the Natural Science Foundation of Zhejiang Province (LQ18B010005), the Research Start-Up Fund of NUAA (90YAH16008), and a project funded by the Priority Academic Program Development of Jiangsu Higher Education Institutions (PAPD). The authors express their appreciations for the above financial support.

Keywords: surface plasmon resonance • ordered mesoporous structure • Au nanoparticles • visible-light photo-catalytic performance • CO_2 reduction

[1] N. S. Lewis, D. G. Nocera, *Natl. Acad. Sci. U. S. A.* **2006**, *103,* 15729–15735.

[2] C. Le Quéré, M. R. Raupach, J. G. Canadell, *Nat. Geosci.* **2009**, *2,* 831–836.

[3] H, Tong, S. Ouyang, Y. Bi, N. Umezawa, M. Oshikiri, J. Ye, *Adv. Mater.* **2012**, *24***,** 229–251.

[4] S. C. Roy, O. K. Varghese, M. Paulose, C. A. Grimes, *ACS Nano* **2010**, *4*, 1259–1278.

[5] H. Pang, T. Masuda, J. Ye, *Chem. Asian J.* **2017**. DOI: 10.1002/asia.201701596.

[6] J. Lin, Dr. Y. Hou, Y. Zheng, X. Wang, *Chem. Asian J.* **2014**, 9, 2468–2474.

[7] G. Zhao, X. Huang, X. Wang and X. Wang, *J. Mater. Chem. A* **2017**, 5, 21625–21649.

[8] W. Wang, S. Wang, X. Ma, J. Gong, *Chem. Soc. Rev.* **2011**, *40***,** 3703–3727.

[9] Q. Liu, Y. Zhou, Z. Tian, X. Chen, J. Gao, Z. Zou, *J. Mater. Chem.* **2012**, *22,* 2033–2038.

[10] S. Yan, H. Yu, N. Wang, Z. Li, Z. Zou, *Chem. Commun.* **2012**, *48*, 1048–1050.

[11] N. Zhang, S. Ouyang, T. Kako, J. Ye, *Chem. Commun.* **2012**, *48,* 1269–1271.

[12] P. Li, H. Xu, L. Liu, T. Kako, N. Umezawa, H. Abe, J. Ye, *J. Mater. Chem. A* **2014**, *2*, 5606–5609.

[13] A. Kudo, Y. Miseki, *Chem. Soc. Rev.* **2009**, *38*, 253–278.

[14] W. Zhou, Y. Guan, D. Wang, X. Zhang, D. Liu, H. Jiang, J. Wang, X. Liu, H. Liu, S. Chen, *Chem. Asian J. **2014**, 9, 1648–1654.*

[15] W. Dai, J. Yan, K. Dai, L. Li, N. Guan, *Chinese J. Catal.* **2015**, 36, 1968–*1975*.

[16] G. Zhang, H. Miao, X. Hu, J. Mu, X. Liu, T. Han, J. Fan, E. Liu, Y. Yin, J. Wan, *Appl. Surf. Sci.* **2017**, 391, 345-352.

[17] Z. Pap, A. Radu, I. Hidi, G. Melinte, L. Diamandescu, T. Popescu, L. Baia, V. Danciu, M. Baia, Chinese J. Catal. **2013**, 34, 734–740.
[18] H. Gong, T. Wang, H. Xue, X. Fan, B. Gao, H. Zhang, L. Shi, J. He, J. Ye, *Energy Storage Materials*, **2018**, 13, 49-56.
[19] G. Xi, S. Ouyang, J. Ye, *Chem. Eur. J.* **2011**, *17,* V9057–V9061.
[20] M. Anpo, H. Yamashita, K. Ikeue, Y. Fujii, S. G. Zhang, V. Y. Ichihashi, D. R. Park, Y. Suzuki, K, Koyano, T. Tatsumi, *Catal. Today* **1998**, *44,* 327–332.
[21] T. Wang, X. Meng, P. Li, S. Ouyang, K. Chang, G. Liu, Z. Mei, J. Ye *Nano Energy* **2014**, *9*, 50-60.
[22] T. Wang, X. Meng, G. Liu, K. Chang, P. Li, Q. Kang, L. Liu, M. Li, S. Ouyang, J. Ye, *J. Mater. Chem. A* **2015**, *3*, 9491-9501.
[23] Y. Noda, B. Lee, K. Domen, J. Kondo, *Chem. Mater.* **2008**, *20*, 5361–5367.
[24] G. S. Li, D. Q. Zhang, J. C. Yu, *Chem. Mater.* **2008**, *20*, 3983–3992.
[25] J. Du, X. Y. Lai, N. L. Yang, J. Zhai, D. Kisailus, F. B. Su, D. Wang, L. Jiang, *ACS Nano* **2011**, *5*, 590–596.
[26] Z. F. Bian, J. Zhu, S. H. Wang, Y. Cao, X. F. Qian, H. X. Li, *J. Phys. Chem. C* **2008**, *112*, 6258–6262.
[27] G. Zhao, Y. Sun, W. Zhou, X. Wang, K. Chang, G. Liu, H. Liu, T. Kako, J. Ye, *Adv. Mater.* **2017,** 29, 1605502.
[28] R. Zhang, X. Wang, S. Yu, T. Wen, X. Zhu, F. Yang, X. Sun, X. Wang and W. Hu, *Adv. Mater.* **2017**, 29, 1605502.
[29] Y. Yang, Z. Ma, L. Xu, H. Wang, N. Fu, *Appl. Surf. Sci.* **2016**, 369, 576-583.
[30] J. Liu, Y. Zhou, F. Han, D. Chen, L. Chen, *Mater. Lett.* **2017**, 207, 109-112.
[31] Z. Zheng, B. Huang, X. Qin, X. Zhang, Y. Dai, M. –H. Whangbo, *J. Mater. Chem.* **2011**, *21***,** 9079–9087.
[32] Z. Lou, Z. Wang, B. Huang, Y. Dai, Synthesis and activity of plasmonic photocatalysts *ChemCatChem* **2014**, *6*, 2456–2476.
[33] S. Linic, P. Christopher, D. B. Ingram, *Nat. Mater.* **2011**, *10*, 911–921.
[34] L. Liu, S. Ouyang, J. Ye, *Angew. Chem. Int. Ed.* **2013**, *52*, 6689–6693.
[35] C. Wang, D. Astruc, *Chem. Soc. Rev.* **2014**, *43*, 7188–7216.
[36] L. Liu, P. Li, B. Adisak, S. Ouyang, N. Umezawa, J. Ye, R. Kodiyath, T. Tanabe, G. V. Ramesh, S. Ueda, H. Abe, *J. Mater. Chem. A* **2014**, *2,* 9875–9882.
[37] A. Primo, A. Corma, H. Garcia, *Phys. Chem. Chem. Phys.* **2011**, *13*, 886–910.
[38] Y. Wang, J. Yu, W. Xiao and Q. Li, *J. Mater. Chem. A* 2014, **2**, 3847-3855.
[39] S. Jo, P. Verma, Y. Kuwahara, K. Mori, W. Choi, H. Yamashita, *J. Mater. Chem. A* 2017, **5**, 21883-21892.
[40] C. Clavero, *Nat. Photonics* **2014**, *8,* 95–103.
[41] H. Inouye, K. Tanaka, I. Tanahashi, K. Hirao, *Phys. Rev. B* **1998**, *57,* 11334–11340.
[42] L. Du, A. Furube, K. Hara, R. Katoh, M. Tachiya, *J. Photochem. Photobiol. C* **2013**, *15,* 21–30.
[43] A. Furube, L. Du, K. Hara, R. Katoh, M. Tachiya, *J. Am. Chem. Soc.* **2007**, *129*, 14852–14853.
[44] Z. Bian, T. Tachikawa, P. Zhang, M. Fujitsuka, T. Majima, *J. Am. Chem. Soc.* **2013**, *136*, 458–465.
[45] G. Liu, T. Wang, W. Zhou, X. G. Meng, H. B. Zhang, H. M. Liu, T. Kako, J. H. Ye, *J. Mater. Chem. C* **2015**, *3*, 7538–7542.
[46] L. Q. Liu, P. Li, T. Wang, H. L. Hu, H. Y. Jiang, H. M. Liu, J, H, Ye, *Chem. Commun.* **2015**, *51*, 2173–2176.
[47] L. Liu, T. D. Dao, R. Kodiyath, Q. Kang, H. Abe, T. Nagao, J. Ye, *Adv. Funct. Mater*. **2014**, *24*, 7754–7762.
[48] K Qian, B. C. Sweeny, A. C. Johnston-Peck, W. Niu, J. O. Graham, J. S. DuChene, J. Qiu, Y. –C. Wang, M. H. Engelhard, D. Su, E. A. Stach, W D. Wei, *J. Am. Chem. Soc.* **2014**, *136*, 9842–9845.
[49] H. R. Xue, J. Q. Zhao, J. Tang, H. Gong, P. He, H. S. Zhou, Y. Yamauchi, J. P. He, *Chem. Eur. J.* **2016**, *22*, 4915–4923.
[50] H. R. Xue, J. Tang, H. Gong, H. Guo, X. L. Fan, T. Wang, J. P. He, Y. Yamauchi, *ACS Appl. Mater. Interfaces* **2016**, *8*, 20766–20771.
[51] W. G. Tu, Y. Zhou, Z. G. Zou, *Adv. Funct. Mater.* **2013**, *23*, 4996–5008.

10.1002/asia.201701807

WILEY-VCH

FULL PAPER

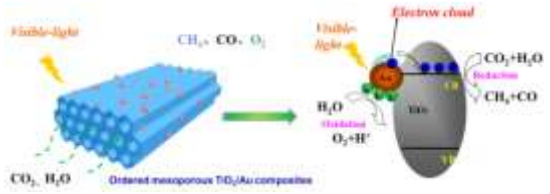

A novel Au-nanoparticle (NP)-decorated ordered mesoporous TiO_2 (OMT) composite (OMT-Au) was successfully fabricated, in which Au NPs uniformly disperse on the OMT. Due to the surface plasmon resonance (SPR) effect derived from the excited Au NPs, TiO_2 possesses high photo-catalytic performance for CO_2 reduction under visible light.

Hairong Xue,[a,b] Tao Wang,[b] Hao Gong,[b] Hu Guo,[b] Xiaoli Fan,[b] Bin Gao,[b] Yaya Feng,[b] Xianguang Meng,[c] and Jianping He*[b]*

Page No. – Page No.

Constructing ordered three-dimensional channels of TiO_2 for enhanced visible-light photo-catalytic performance of CO_2 conversion induced by Au nanoparticles